Chemical Physics Letters 468 (2009) 46–51

Contents lists available at ScienceDirect

Chemical Physics Letters

journal homepage: www.elsevier.com/locate/cplett

Triplet state relaxation processes of the OLED emitter Pt(4,6-dFppy)(acac)

Andreas F. Rausch [a], Mark E. Thompson [b], Hartmut Yersin [a,*]

[a] Universität Regensburg, Institut für Physikalische und Theoretische Chemie, 93053 Regensburg, Germany
[b] University of Southern California, Department of Chemistry, Los Angeles, CA 90089, United States

ARTICLE INFO

Article history:
Received 21 October 2008
In final form 22 November 2008
Available online 3 December 2008

ABSTRACT

The emitting triplet state of Pt(4,6-dFppy)(acac) doped into *n*-octane is studied at cryogenic temperatures by site-selective high-resolution optical spectroscopy. The investigations reveal a very specific zero-field splitting (ZFS) pattern of the emitting T_1 state and the individual deactivation times of the substates to the singlet ground state S_0. Spin-lattice relaxation (SLR) processes occurring between the T_1 substates are ascribed to a combination of the *direct* and the *Raman process*. Due to the relatively long SLR time at low temperature, a Boltzmann distribution is not established directly after the excitation pulse below ≈2 K.

1. Introduction

Phosphorescent organo-transition metal compounds are in the focus of scientific and industrial interest due to their applicability as efficient emitters in organic light emitting diodes (OLEDs) [1–5]. Due to strong spin–orbit coupling induced by the heavy metal center, devices incorporating such triplet emitting materials can exhibit a four times higher internal electroluminescence quantum yield than achievable with fluorescent emitters due to the triplet harvesting effect [4,5].

The most frequently applied central metal ions in phosphorescent OLED emitters are Pt(II) and Ir(III). In contrast to quasi-octahedral Ir(III) compounds, quasi-planar Pt(II) complexes can offer additional possibilities for the generation of light. Due to a strong tendency to form aggregates of electronically strongly interacting monomers, many Pt(II) compounds exhibit an additional broad and red-shifted band compared to the monomer emission [6–10]. For the target compound Pt(4,6-dFppy)(acac) (platinum(II)[2-(4′,6′-difluorophenyl)pyridinato-N,C2]-acetylacetonate, see inset of Fig. 1), a balanced combination of the blue–green monomer emission and the red aggregate emission covers a large spectral range of the visible light [9]. Thus, the aggregate formation has been investigated in detail [11,12] and utilized for efficient white light emitting OLEDs [9,13–16]. For example, a device with a power efficiency of 12.6 lm/W and an external quantum efficiency of 15.9% at 500 cd/m^2, applying the host material 26mCPy (2,6-bis(N-carbazolyl)pyridine), was reported [16].

In this investigation, we study the emitting triplet state T_1 of the Pt(4,6-dFppy)(acac) monomer in an *n*-octane matrix at cryogenic temperatures. Highly resolved emission and excitation spectra at different temperatures and application of external magnetic fields reveal a very specific splitting pattern of the triplet substates and give the magnitude of zero-field splitting (ZFS). This allows us to characterize the T_1 state. A temperature dependent analysis of the decay behavior in the temperature range from 1.2 K to 130 K gives information on the individual deactivation rates of the T_1 substates and reveals interesting spin-lattice relaxation (SLR) effects which determine the relaxation dynamics occurring between the T_1 sublevels at low temperatures.

2. Experimental

Pt(4,6-dFppy)(acac) was synthesized according to the procedure described in Ref. [17].

Spectroscopic measurements were carried out with Pt(4,6-dFppy)(acac) dissolved in *n*-octane with a concentration of about 10^{-5} mol/L. Emission spectra at 300 K were measured with a steady-state fluorescence spectrometer (Jobin Yvon Fluorolog 3). The experiments at low temperatures were carried out in a He cryostat (Cryovac Konti Cryostat IT) in which the He gas flow, He pressure, and heating were controlled. A pulsed Nd:YAG laser (IB Laser Inc., DiNY pQ 02) with a pulse width of about 7 ns was applied as excitation source for decay measurements, using the third harmonic at 355 nm (28170 cm^{-1}). For the recording of site-selective emission and excitation spectra, a pulsed dye laser (Lambdaphysik Scanmate 2C) was operated, using Coumarin 102 and Coumarin 120, respectively. The spectra were measured with an intensified CCD camera (Princeton PIMAX) or a cooled photomultiplier (RCA C7164R) attached to a triple spectrograph (S&I Trivista TR 555). Decay times were registered using a FAST Comtec multichannel scaler PCI card with a time resolution of 250 ps.

* Corresponding author. Fax: +49 941 943 4488.
E-mail address: hartmut.yersin@chemie.uni-regensburg.de (H. Yersin).

0009-2614/$ - see front matter © 2008 Elsevier B.V. All rights reserved.
doi:10.1016/j.cplett.2008.11.075

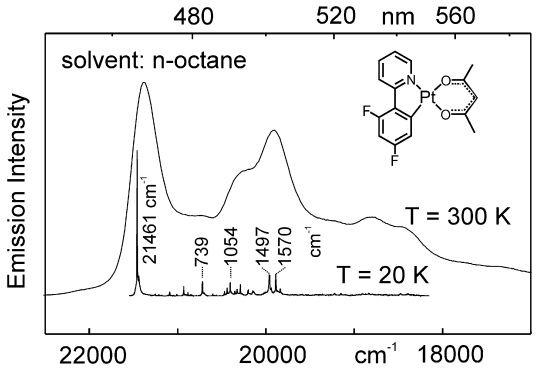

Fig. 1. Comparison of the emission spectra of Pt(4,6-dFppy)(acac) in *n*-octane ($c \approx 10^{-5}$ mol/L) at $T = 300$ K ($\lambda_{exc} = 370$ nm) and at $T = 20$ K. The 20 K spectrum represents the emission of a dominant site, which was excited selectively at 22 161 cm^{-1} ($0 \rightarrow II/III + 700\ cm^{-1}$ vibration). The energies of some prominent vibrational satellites are also given.

3. Results and discussion

3.1. Spectroscopic situation – selective excitation at low temperatures

A discussion of spectroscopic properties of Pt(4,6-dFppy)(acac) at ambient temperature is presented in the Refs. [12,17]. However, a detailed investigation of the emitting T_1 state is not feasible on the basis of broadband spectra at room temperature. Therefore, the compound was dissolved in *n*-octane at low concentration and cooled to cryogenic temperatures. In this polycrystalline matrix, the guest molecules (dopants) substitute host molecules and lie at defined positions. Application of this so-called Shpol'skii technique [18] results in highly resolved spectra with linewidths of only a few cm^{-1} due to a residual inhomogeneity. The obtained line widths are by a factor of hundred smaller than usually obtained with amorphous or glassy host materials. Mostly, the observed spectra in Shpol'skii matrices represent a superposition of spectra stemming from several sites. However, by selective excitation with a tunable dye laser it is possible to investigate just one specific site. Fig. 1 compares the selectively excited emission spectrum of a dominant site of Pt(4,6-dFppy)(acac) in *n*-octane, measured at $T = 20$ K, to the 300 K spectrum in the same solvent.

The ambient temperature spectrum consists of overlapping and broadened bands with halfwidths of about 500 cm^{-1}, while the emission spectrum at $T = 20$ K exhibits narrow lines with halfwidths of 4 cm^{-1}. It will be shown below that the most intense line in the highly resolved spectrum depicted in Fig. 1 represents the purely electronic 0–0 transition from the two higher lying T_1 substates II and III to the singlet ground state S_0. The lines of minor intensity correspond to vibrational satellites. Some representative values measured with respect to the electronic 0–0 transition at 21 461 cm^{-1} are also given. Due to the high intensity of the electronic origin compared to the weak satellites, it can be concluded that the purely electronic 0–0 transitions $II/III \rightarrow 0$ are induced by direct spin–orbit coupling and that the vibrational satellites occurring at $T = 20$ K stem mostly from Franck–Condon activity [19–21]. This is further supported by the observation of weak progressions of several of these satellites [22,23]. A more detailed analysis of the vibrational satellite structure is presented in Ref. [23]. In the present investigation, we focus on an analysis of the electronic 0–0 transitions, the corresponding states, and the involved relaxation properties.

3.2. Electronic origins – temperature and magnetic field dependence

At $T = 20$ K, only one electronic 0–0 transition is observed (Fig. 1). To gain more detailed information on the different transitions between the T_1 substates and the singlet ground state S_0, emission and excitation measurements have to be carried out at different temperatures and high magnetic fields. Fig. 2 shows the corresponding spectra for the region of the electronic origins.

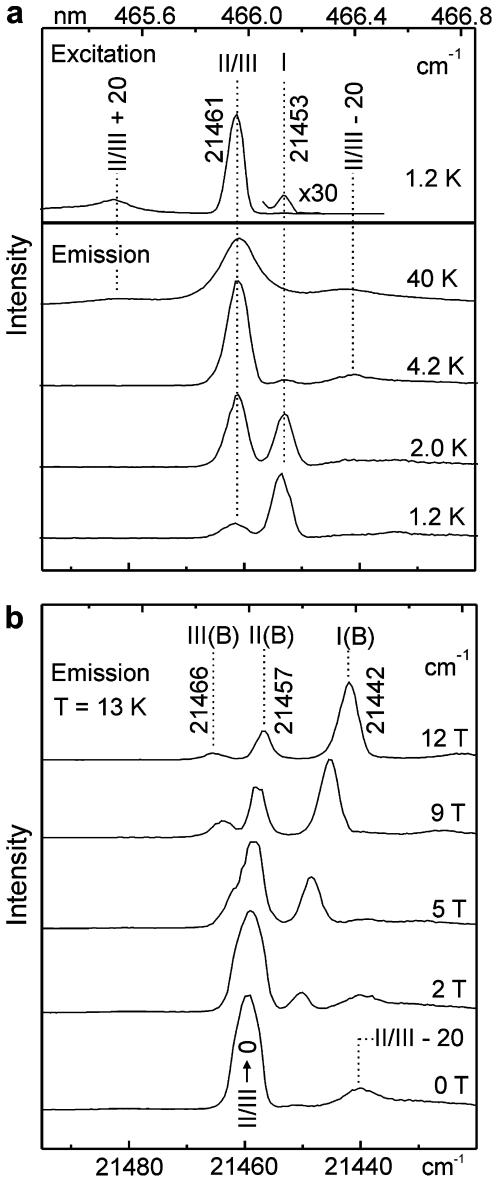

Fig. 2. (a) Emission and excitation spectra of Pt(4,6-dFppy)(acac) in *n*-octane ($c \approx 10^{-5}$ mol/L) at selected temperatures. For the excitation spectrum, the emission was detected at an energy of 21 012 cm^{-1}, which corresponds to a vibrational satellite of the transition I → 0 (441 cm^{-1} vibration). The emission spectra were recorded after selective excitation into a vibrational satellite of the transition 0 → II/III at 22 161 cm^{-1} (700 cm^{-1} vibration). (b) Emission spectra at $T = 13$ K at different magnetic field strengths. The sample was selectively excited into the 700 cm^{-1} vibrational satellite of the transition 0 → II(B). The energy values given in (a) and (b) are rounded to 1 cm^{-1} corresponding to the accuracy of the absolute wavenumber. The relative accuracy is as high as ±0.3 cm^{-1}.

Fig. 2a shows that, at $T = 1.2$ K, the line at 21 453 cm^{-1} is the most intense one in the emission spectrum. This low-energy line is assigned as electronic 0–0 transition I → 0 from the lowest T_1 substate I to the singlet ground state 0. A second, weaker line lies at 21 461 cm^{-1}. With temperature increase, it gains intensity and slightly broadens. It will be shown below that this line represents the electronic 0–0 transitions from the two higher lying T_1 substates II and III to the ground state. The purely electronic nature of the lines at 21 453 cm^{-1} and 21 461 cm^{-1} is substantiated by

the fact that the corresponding transitions appear resonantly in emission and in excitation at low temperature. From the intensity ratio of the lines observed in excitation, it can be concluded that the transition 0 → II/III is by a factor of 190 ± 10 more allowed than the transition 0 → I and thus, carries a significantly higher oscillator strength (note the scaling factor in Fig. 2a). The additional lines observed in Fig. 2a, occurring 20 cm^{-1} lower (higher) in energy in emission (excitation) with respect to the line at 21 461 cm^{-1} represent local phonon satellites due to vibrations of the dopant in its matrix cage. The high energy phonon is also found in the 40 K emission spectrum as hot band. Local phonon satellites of similar energy are frequently observed [19,24].

The fact that the line at 21 461 cm^{-1} corresponds to two T_1 substates is revealed under the application of high magnetic fields. Fig. 2b displays the emission spectra at T = 13 K for magnetic fields up to B = 12 T. Due to the Zeeman effect, the wavefunctions of the three T_1 sublevels mix and a significant splitting of the substates II/III is obtained. The corresponding lines, lying in an energy range of <1 cm^{-1} at zero-field, exhibit a splitting of (8.7 ± 0.3) cm^{-1} at B = 12 T. The temperature of 13 K was chosen to provide a thermal population of all three substates also under application of high B-fields. The Zeeman mixing does not only split the substates II and III, but causes also an increase of the total splitting. While it amounts to $\Delta E_{II/III-I}$ = (8.3 ± 0.3) cm^{-1} at B = 0 T, a value of $\Delta E_{III-I}(B)$ = (23.6 ± 0.3) cm^{-1} is observed at B = 12 T. Moreover, due to the field-induced mixings between the substates, the emission from the lowest B-field perturbed substate I(B) becomes dominant and the transitions II(B) → 0 and III(B) → 0 lose intensity with increasing magnetic field. This behavior shows that the magnetic field distinctly alters the properties of the respective 0–0 transitions.

3.3. Thermalized emission decay and energy level diagram

At zero magnetic field, the transitions I ↔ 0 and II/III ↔ 0 exhibit distinctly different oscillator strengths. This behavior is expected to be manifested also in the emission decay of the respective T_1 substates. Emission decay curves measured at T = 1.2 K are shown for a detection energy of 21 453 cm^{-1} (electronic 0–0 transition I → 0) in Fig. 3a and for a detection energy of 21 461 cm^{-1} (electronic 0–0 transition II/III → 0) in Fig. 3b.

Detection of the emission decay at the I → 0 transition gives a monoexponential decay with a time constant of 85 μs (Fig. 3a). In contrast, monitoring the emission decay at the II/III → 0 transition leads to a bi-exponential curve with time constants of 240 ns and 85 μs. The long component, found in both curves, represents the thermalized emission decay from the three T_1 substates, while the short component is dominated by relaxation processes from the substates II/III to substate I (spin-lattice relaxation). This phenomenon will be further investigated in Section 3.4. The individual emission decay times of the substates to the ground state cannot be recorded directly, since at higher temperatures usually the thermalized emission of all three substates is measured. However, these individual decay times can still be determined from the temperature dependence of the thermalized emission decay. In Fig. 3c, the measured values are plotted versus temperature for the range 1.2 K ⩽ T ⩽ 130 K. For a thermally equilibrated system of three excited states of which the two higher lying states are considered as energetically nearly degenerate, the thermalized emission decay time τ_{therm} is given by the expression (compare e.g. Refs. [25–28])

$$\tau_{therm} = \frac{1 + 2 \cdot \exp\left(\frac{-\Delta E_{II/III-I}}{k_B T}\right)}{k_I + k_{II/III} \cdot \exp\left(\frac{-\Delta E_{II/III-I}}{k_B T}\right)} \quad (1)$$

wherein k_I and $k_{II/III}$ are the rate constants for the depopulation of the substates I and II/III, and $\Delta E_{II/III-I}$ represents the energy separation between the respective substates. It is assumed that $\Delta E_{II-I} \approx \Delta E_{III-I} = \Delta E_{II/III-I}$ and that $k_{II/III} = k_{II} + k_{III}$ represents the combined rate constant of depopulation of the substates II and III. A fitting procedure, using the experimental decay time data and Eq. (1), provides individual decay times of τ_I = (85.0 ± 0.5) μs, $\tau_{II/III}$ = (2.6 ± 0.2) μs and an energy separation of $\Delta E_{II/III-I}$ = (8.5 ± 0.5) cm^{-1}. The latter value is in good agreement with the splitting of 8.3 cm^{-1} obtained from highly resolved spectra (see Section 3.2). Interestingly, the value for τ_I given by the fit corresponds to the measured long decay component at T = 1.2 K. Thus, no significant thermal repopulation of the higher lying T_1 substates II/III is expected at this temperature. It will be shown below that the emission from these higher lying states, as observed at temperatures below ≈2 K (Fig. 2a), mainly stems from an initial population after the excitation pulse followed by a relatively slow thermalization (relaxation).

For completeness, it is remarked that the rate constant for $k_{II/III} = 1/\tau_{II/III} = 3.84 \times 10^5\ s^{-1}$, as determined by the fitting procedure, is only by a factor of ≈32 higher than the rate constant $k_I = 1/\tau_I = 1.2 \times 10^4\ s^{-1}$ This result does not contradict to the value of 190, as obtained from the intensity ratio of the purely electronic 0–0 transitions observed in the highly resolved excitation spec-

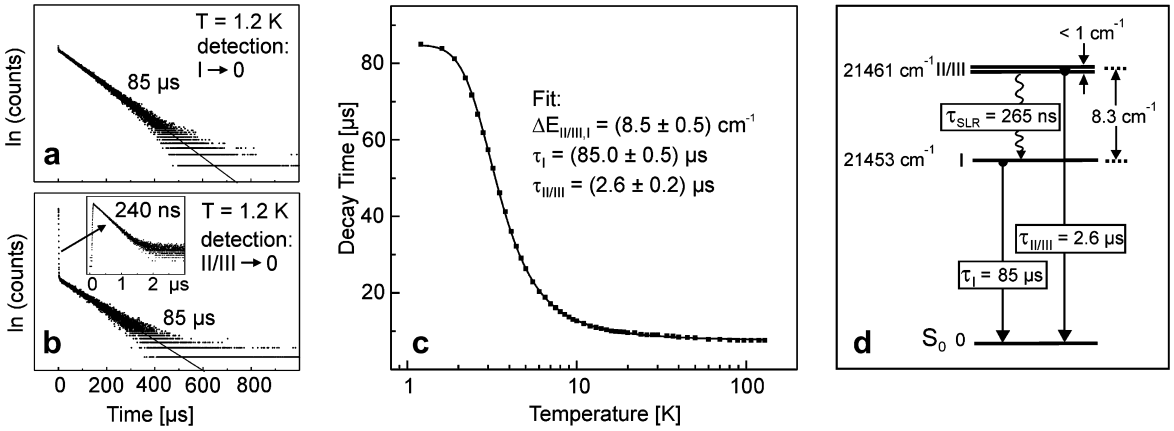

Fig. 3. Emission decay properties of Pt(4,6-dFppy)(acac) in *n*-octane at after excitation at 355 nm and energy level diagram. (a) Decay at T = 1.2 K for a detection at the electronic 0–0 transition I → 0 (21 453 cm^{-1}). (b) Decay at T = 1.2 K for a detection at the electronic 0–0 transition II/III → 0 (21 461 cm^{-1}). The short component of the bi-exponential decay is displayed in the inset on an enlarged scale. (c) Plot of the thermalized emission decay time versus temperature. For temperatures of T ⩽ 2 K, the emission was detected at the energy of the 0–0 transition I → 0, while, for T > 2 K, a detection at the energy of the 0–0 transition II/III → 0 was chosen. The solid line represents a fit of Eq. (1) to the experimental data. The results obtained from the fit are shown in the inset. (d) Energy level diagram. The energy difference $\Delta E_{II/III-I}$ is obtained from highly resolved spectra. The spin-lattice relaxation time of τ_{SLR} = 265 ns is derived in Section 3.4.

trum. (Section 3.2) Both values are only comparable, if the respective substates exhibit identical deactivation paths. For Pt(4,6-dFppy)(acac), however, it has been shown that the vibrational satellites in the emission of the substates II/III stem dominantly from Franck–Condon activity, while the deactivation of substate I is largely based on Herzberg–Teller vibronic activity [23]. This means that the radiative deactivation mechanisms of the substates II/III and I, respectively, differ strongly. (For a detailed description of the corresponding mechanisms compare Ref. [19]).

The results obtained allow us to derive the energy level diagram for the T_1 substates as shown in Fig. 3d. The spin-lattice relaxation time of $\tau_{SLR} = 265$ ns occurring between the substates II/III and I will be discussed in the next section. The energy separation of $\Delta E_{II/III\text{-}I} = 8.3\ cm^{-1}$, i.e. the total zero-field splitting, can be used to classify the emitting triplet state. This value indicates the amount of MLCT (metal-to-ligand charge transfer) character and the importance of spin–orbit coupling (SOC) for the emitting triplet state via the involved d-orbital character. Effective SOC with higher lying singlet MLCT states is necessary to induce a significant radiative emission decay rate from a triplet substate to the singlet ground state [23,24,29]. The extremely weak allowedness observed for the transition $0 \rightarrow I$ (Fig. 2a) and the long decay time of $\tau_I = 85$ μs indicate that substate I exhibits almost pure triplet character, while the substates II/III with $\tau_{II/III} = 2.6$ μs and a much higher allowedness for the transitions $0 \rightarrow II/III$ (Fig. 2a) contain significant admixtures of higher lying ^{1}MLCT states. In conclusion and according to an empirical ordering scheme [5,24,30], a triplet state which exhibits a value of $\Delta E(ZFS) = 8\ cm^{-1}$ can be assigned as being largely ligand centered (^{3}LC, $^3\pi\pi^*$) with only moderate MLCT ($5d\pi^*$) perturbations.

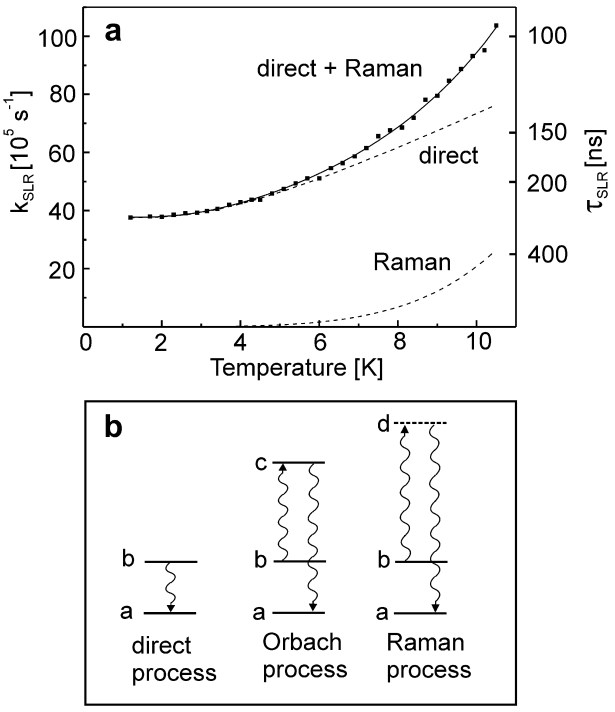

Fig. 4. (a) Rate of spin-lattice relaxation between the T_1 substates II/III and I of Pt(4,6-dFppy)(acac) in *n*-octane versus temperature. The solid line represents a fit to the experimental data according to Eq. (3), i.e. to the *direct process* and the *Raman process*. The individual contributions of each process are also displayed. (b) Schematic illustration of processes of SLR.

3.4. Spin-lattice relaxation – temperature dependence

At low temperature, the emission of the triplet substates II/III exhibits a bi-exponential decay. For example, at $T = 1.2$ K, the short-time component amounts to $\tau^{exp}_{II/III} = 240$ ns and the long-time component to $\tau_{therm} = 85$ μs (Fig. 3b). The occurrence of the short component is related to processes of spin-lattice relaxation (SLR) (compare Ref. [30]). These relaxation times can be relatively long when the energy separations between the involved substates are only several wavenumbers or less, since the excess energy of a higher lying triplet sublevel is not easily transferred to the lattice due to the small density of states of lattice vibrations (phonons) in this energy range [19,20,30].

The substates II/III are depopulated by relaxations to substate I, given by the SLR rate $k_{SLR} = (\tau_{SLR})^{-1}$, and to the ground state 0, given by the usual decay rate $k_{II/III} = (\tau_{II/III})^{-1}$. The experimentally determined decay rate (short component) can be expressed by Eq. (2) [19,30,31].

$$k^{exp}_{II/III} = \frac{1}{\tau^{exp}_{II/III}} = k_{SLR} + k_{II/III} \tag{2}$$

With $\tau^{exp}_{II/III} = 240$ ns and $k_{II/III} = \tau^{-1}_{II/III} = (2.6\ \mu s)^{-1}$ (Section 3.3) a value of $\tau_{SLR} = 265$ ns is found for $T = 1.2$ K (Fig. 3d).

With temperature increase, the SLR rate k_{SLR} increases for Pt(4,6-dFppy)(acac) in *n*-octane in the investigated range $1.2\ K \leqslant T \leqslant 10.5\ K$ as shown in Fig. 4a. For a description of this temperature dependence, three different processes have to be considered [19,30,32,33]. They are schematically depicted in Fig. 4b.

The *direct process* involves the emission of one phonon of the energy $\Delta E_{b\text{-}a}$, which is transmitted to the lattice. The rate of this process usually dominates at low temperatures and exhibits only a moderate temperature dependence. At higher temperatures, the relaxation may also proceed indirectly via the *Orbach process*, which represents a two-phonon process by involving a third real state *c*. Here, one phonon of the energy $\Delta E_{c\text{-}b}$ is absorbed, while a second phonon of the energy $\Delta E_{c\text{-}a}$ is emitted. The *Raman process* is also a two-step process and occurs under the involvement of a virtual level *d*. In analogy to the optical Raman process, it can be described as inelastic phonon scattering process.

For the case of Pt(4,6-dFppy)(acac) in *n*-octane, the spin-lattice relaxation occurs between the energetically very proximate substates II/III and substate I. Since no evidence for a further higher lying state is given, it is indicated that only the *direct* and the *Raman process* are significant [20,30,32]. Thus, the temperature dependence of the SLR rate can be expressed by [32]

$$k_{SLR} = C_{II/III\text{-}I} \times (\Delta E_{II/III\text{-}I})^3 \times \coth\left(\frac{\Delta E_{II/III\text{-}I}}{2k_B T}\right) + R \times T^n. \tag{3}$$

The constant $C_{II/III\text{-}I}$ can also be written as $C_{III\text{-}I} + C_{II\text{-}I}$, which contain quantities such as the matrix density of states, the velocity of sound in the matrix and the square of the respective coupling matrix element [19,20]. *n* is a parameter which is regarded to be 5 for this type of compounds [34,32] and was kept fixed during the fitting procedure. Eq. (3) can be fit nicely to the experimental data (Fig. 4a). The individual contributions from the two different SLR processes taken into account are also displayed graphically. Up to a temperature of about 5 K, k_{SLR} can be described only by the *direct process*. With further temperature increase, the *Raman process* becomes also important and has to be included for an accurate fit. Note that, even at $T = 10.5$ K, the direct process provides the largest contribution to the SLR rate.

From the fitting procedure the parameters $C_{II/III\text{-}I} = (7700 \pm 200)\ cm^3 s^{-1}$, $R = (21 \pm 1)\ s^{-1}\ K^{-5}$, and $\Delta E_{II/III\text{-}I} = (7.9 \pm 0.5)\ cm^{-1}$ are obtained. The energy separation agrees well with the value obtained from highly resolved spectra (see Section 3.2). If one allows for a free fit of the exponent *n* of the T^n power law that describes the *Raman process*, a value of $n = (4.4 \pm 0.7)$ is obtained. Moreover,

a fit with a T^7 dependence – as observed for other systems [35–37] – is not consistent with the experimental data. Thus, the present case study represents another example of an organo-transition metal compound for which the $n = 5$ exponent seems to be well suited (compare Refs. [19,30,32]).

It is remarked that an additional implementation of the *Orbach process* does not provide any further improvement of the fit. This supports the assumption that no higher lying electronic state in the thermally accessable energy range is present. For compounds with an additional higher lying T_1 substate, such as $Pt(2\text{-thpy})_2$ (2-thpy$^-$ = 2-(2-thienyl)-pyridinate) [19,32], $Ir(btp)_2(acac)$ (btp$^-$ = (2-benzothienyl)-pyridinate) [31], and $[Ru(bpy)_3]^{2+}$ (bpy = 2,2′-bipyridine) [30,38] the temperature dependence of SLR cannot be described by Eq. (3), since the involvement of the *Orbach process* is indispensable.

3.5. Effects of spin-lattice relaxation on the substate population

The discussion as presented in Section 3.4 has demonstrated that the sublevels II/III and I of the T_1 state of Pt(4,6-dFppy)(acac) in *n*-octane are at sufficiently low temperature not in a thermal equilibrium. Thus, it is not expected that, in the respective temperature range, the population of these states can be described by a Boltzmann distribution, which is based on thermally equilibrated states [26,27]. The deviation becomes obvious when the temperature dependence of the emission intensity ratio is analyzed for the electronic 0–0 transitions II/III → 0 and I → 0. Fig. 5a shows a plot of $\ln(Int_{II/III}(ti)/Int_I(ti))$ versus $\Delta E_{II/III\text{-}I}/k_BT$, wherein $Int_{II/III}(ti)$ and $Int_I(ti)$ represent the time integrated emission intensities of the corresponding 0–0 transitions (compare also Fig. 2a).

At temperatures below ≈2 K, a clear deviation from a straight line and thus from a Boltzmann distribution is observed. This is a consequence of the fact that the emission from the higher lying substates II/III cannot be frozen out (see Fig. 2a). For example, at $T = 1.2$ K, the 0–0 transition II/III → 0 is more intense than expected from a Boltzmann behavior, since after the initial population of the substates II/III the relaxation to substate I is comparatively slow (265 ns). At temperatures between about 2 K and 3 K the rate constant of SLR is still of similar size (Fig. 4a), but now the thermal equilibration dominates the effects of SLR. Thus, the deviation from a Boltzmann distribution is no longer distinct above 2 K.

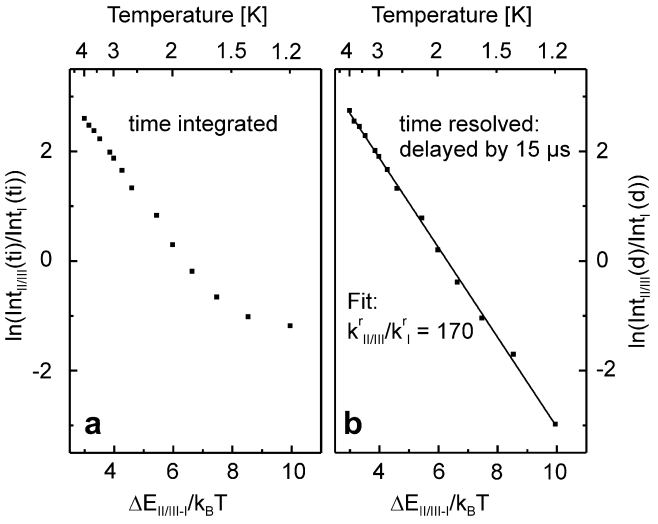

Fig. 5. Boltzmann plots of the emission intensity ratios of the electronic 0–0 transitions II/III → 0 and I → 0 versus $\Delta E_{II/III\text{-}I}/k_BT$ for Pt(4,6-dFppy)(acac) in *n*-octane after selective excitation at 22 161 cm^{-1} (0–0 transition 0 → II/III + 700 cm^{-1} vibration). The ratios shown in (a) result from time integrated spectra, while the ratios depicted in (b) are derived from time delayed spectra with a delay time of 15 µs after the exciting laser pulse and a time window of 500 µs. The data in the delayed spectrum (b) are nicely fit by Eq. (4).

According to the above discussion, the thermal equilibration directly after the exciting laser pulse is not obtained at low temperature. However, after an appropriate delay time, for example after several µs, thermal equilibrium should be established. Indeed, the intensity ratio as determined after a delay time of 15 µs (Fig. 5b) follows the Boltzmann distribution and can be fit by the equation

$$\frac{Int_{II/III}(d)}{Int_I(d)} = \frac{k^r_{II/III}}{k^r_I} \cdot \exp\left(-\frac{\Delta E_{II/III\text{-}I}}{k_BT}\right). \quad (4)$$

$k^r_{II/III}$ and k^r_I are the radiative rates of the corresponding purely electronic transitions and $Int_{II/III}(d)$ and $Int_I(d)$ represent the corresponding emission intensities. From a fit of Eq. (4) to the data given in Fig. 5b a value of $k^r_{II/III}/k^r_I = (170 \pm 10)$ is determined. Within the limit of experimental error this value matches well with the oscillator strength ratio of (190 ± 10) derived in Section 3.2. This result indicates that – at least in the temperature range between 1.2 K and 4 K – nonradiative processes are negligible for the electronic 0–0 transitions II/III → 0 and I → 0.

4. Summary and conclusions

The lowest triplet state of Pt(4,6-dFppy)(acac) in *n*-octane has been characterized in detail at cryogenic temperatures with respect to the zero-field splitting (ZFS) of the T_1 state, the decay behavior of the transitions to the ground state, and the dynamics of spin-lattice relaxation between the T_1 substates. Highly resolved emission and excitation spectra reveal a total zero-field splitting of $\Delta E_{II/III\text{-}I} = 8.3$ cm^{-1} with a small energy separation of $\Delta E_{III\text{-}II} < 1$ cm^{-1} between the two higher lying T_1 substates. The ΔE(ZFS) value of the T_1 state of Pt(4,6-dFppy)(acac) is about one order of a magnitude smaller than the T_1 state splittings of the Ir(III) compounds $Ir(4,6\text{-dFppy})_2(pic)$ (FIrpic) [23,39] and $Ir(4,6\text{-dFppy})_2(acac)$ [40].

An equivalent behavior is frequently found, i.e. square-planar organo-transition metal compounds often exhibit much smaller ZFS values than equivalent octahedral complexes. This tendency is explained by specific differences in spin–orbit coupling (SOC) to higher lying ^{1}MLCT and ^{3}MLCT states. These coupling routes can in general be more effective in (distorted) octahedral than in (distorted) square-planar compounds [23,24].

The size of the total zero-field splitting displays the character of the T_1 state. Large ZFSs can only result from efficient SOCs to higher lying ^{1,3}MLCT states, while such couplings to $^{1,3}\pi\pi^*$ states are weak [23,24,29,41]. Thus, it can be concluded that the emitting T_1 state of Pt(4,6-dFppy)(acac) is largely of ^{3}LC ($\pi\pi^*$) character with only small MLCT ($5d\pi^*$) contributions. More detailed discussions and systematics in this respect are found in Refs. [19,23,24,30].

The specific ZFS pattern as observed for Pt(4,6-dFppy)(acac), exhibiting two higher lying triplet substates of very proximate energy with the third substate being distinctly stabilized, is only rarely observed [42,43]. This behavior is related to specific SOC routes to higher lying states. Since such routes determine the radiative properties of triplet emitters, such as emission decay time and emission quantum yield, a deeper understanding of individual splitting patterns and SOC routes is highly desired. Corresponding investigations might lead to the possibility of a more systematic chemical engineering of efficient triplet emitters to be applied in OLEDs. However, further detailed experimental studies and theoretical investigations under inclusion of SOC are required.

Acknowledgments

We thank the *Bundesministerium für Bildung und Forschung (BMBF)* for the funding of our research. The *BaCaTeC* is acknowledged for financial support of the exchange program of the University of Regensburg with the University of Southern California.

References

[1] H. Yersin (Ed.), Highly Efficient OLEDs with Phosphorescent Materials, Wiley-VCH, Weinheim, 2008.
[2] B. Hirani, J. Li, P.I. Djurovich, M. Yousufuddin, J. Oxgaard, P. Persson, S.R. Wilson, R. Bau, W.A. Goddard, III, M.E. Thompson, Inorg. Chem. 46 (2007) 3865.
[3] S.-J. Su, H. Sasabe, T. Takeda, J. Kido, Chem. Mater. 20 (2008) 1691.
[4] C. Adachi, M.A. Baldo, M.E. Thompson, S.R. Forrest, J. Appl. Phys. 90 (2001) 5048.
[5] H. Yersin, Top. Curr. Chem. 241 (2004) 1.
[6] W.B. Connick, D. Geiger, R. Eisenberg, Inorg. Chem. 38 (1999) 3264.
[7] C.N. Pettijohn, E.B. Jochnovitz, B. Chuong, J.K. Nagle, A. Vogler, Coord. Chem. Rev. 171 (1998) 85.
[8] J.A.G. Williams, A. Beeby, E.S. Davies, J.A. Weinstein, C. Wilson, Inorg. Chem. 42 (2003) 8609.
[9] V. Adamovich, J. Brooks, A. Tamayo, A.M. Alexander, P.I. Djurovich, B.W. D'Andrade, C. Adachi, S.R. Forrest, M.E. Thompson, New. J. Chem. 26 (2002) 1171.
[10] H. Yersin, D. Donges, W. Humbs, R. Sitters, M. Glasbeek, Inorg. Chem. 41 (2002) 4515.
[11] B. D'Andrade, S.R. Forrest, Chem. Phys. 286 (2003) 321.
[12] B. Ma, P.I. Djurovich, M.E. Thompson, Coord. Chem. Rev. 249 (2005) 1501.
[13] B.W. D'Andrade, J. Brooks, V. Adamovich, M.E. Thompson, S.R. Forrest, Adv. Mater. 14 (2002) 1032.
[14] B.W. D'Andrade, S.R. Forrest, J. Appl. Phys. 94 (2003) 3101.
[15] V.I. Adamovich, S.R. Cordero, P.I. Djurovich, A. Tamayo, M.E. Thompson, B.W. D'Andrade, S.R. Forrest, Org. Electron. 4 (2003) 77.
[16] E.L. Williams, K. Haavisto, J. Li, G.E. Jabbour, Adv. Mater. 19 (2007) 197.
[17] J. Brooks, Y. Babayan, S. Lamansky, P.I. Djurovich, I. Tsyba, R. Bau, M.E. Thompson, Inorg. Chem. 41 (2002) 3055.
[18] E.V. Shpol'skii, Sov. Phys. Usp. (Engl. Transl.) 3 (1960) 372.
[19] H. Yersin, D. Donges, Top. Curr. Chem. 214 (2001) 81.
[20] B. Henderson, G.F. Imbusch, Optical Spectroscopy of Inorganic Solids, Clarendon, Oxford, 1989.
[21] R.M. Hochstrasser, Molecular Aspects of Symmetry, W.A. Benjamin Inc., New York, 1966.
[22] A.F. Rausch, Ph.D. thesis, Universität Regensburg, in preparation.
[23] A.F. Rausch, H.H.H. Homeier, P.I. Djurovich, M.E. Thompson, H. Yersin, in: Z. Kafafi, F. So (Eds.), Proc of SPIE Optics and Photonics – Organic Light Emitting Materials and Devices XI, vol. 6655, San Diego, USA, 2007, p. 66550F.
[24] H. Yersin, W.J. Finkenzeller, in: H. Yersin (Ed.), Highly Efficient OLEDs with Phosphorescent Materials, Wiley-VCH, Weinheim, 2008, p. 1.
[25] W.J. Finkenzeller, H. Yersin, Chem. Phys. Lett. 377 (2003) 299.
[26] R.W. Harrigan, G.A. Crosby, J. Chem. Phys. 59 (1973) 3468.
[27] T. Azumi, C.M. O'Donnell, S.P. McGlynn, J. Chem. Phys. 45 (1966) 2735.
[28] D. Pentlehner, I. Grau, H. Yersin, Chem. Phys. Lett. 455 (2008) 72.
[29] Z. Abedin-Siddique, T. Ohno, K. Nozaki, Inorg. Chem. 43 (2004) 663.
[30] H. Yersin, J. Strasser, Coord. Chem. Rev. 208 (2000) 331.
[31] W.J. Finkenzeller, M.E. Thompson, H. Yersin, Chem. Phys. Lett. 444 (2007) 273.
[32] J. Strasser, H.H.H. Homeier, H. Yersin, Chem. Phys. 255 (2000) 301.
[33] H.H.H. Homeier, J. Strasser, H. Yersin, Chem. Phys. Lett. 316 (2000) 280.
[34] M.B. Walker, Can. J. Phys. 46 (1968) 1347.
[35] P.L. Scott, C.D. Jeffries, Phys. Rev. 127 (1962) 32.
[36] L.H. Hall, M.A. El-Sayed, Chem. Phys. 8 (1975) 272.
[37] A. Abragam, B. Bleanney, Electron Paramagnetic Resonance of Transition Ions, Clarendon, Oxford, 1970.
[38] H. Yersin, W. Humbs, J. Strasser, Top. Curr. Chem. 191 (1997) 153.
[39] A.F. Rausch, M.E. Thompson, H. Yersin, Inorg. Chem., in press.
[40] A.F. Rausch, M.E. Thompson, H. Yersin, submitted for publication.
[41] H. Miki, M. Shimada, T. Azumi, J.A. Brozik, G.A. Crosby, J. Phys. Chem. 97 (1993) 11175.
[42] A.F. Rausch, Diplomarbeit, Universität Regensburg, 2006.
[43] T. Hofbeck, Diplomarbeit, Universität Regensburg, 2007.